DSCC2017-5349

LOCOMOTION OF A MULTI-LINK NONHOLONOMIC SNAKE ROBOT

Tony Dear*

Robotics Institute Carnegie Mellon University Pittsburgh, Pennsylvania 15213 tonydear@cmu.edu

Scott David Kelly

Department of Mechanical Engineering and Engineering Science University of North Carolina at Charlotte Charlotte, North Carolina 28223 scott@kellyfish.net

Matthew Travers Howie Choset

Robotics Institute
Carnegie Mellon University
Pittsburgh, Pennsylvania 15213
mtravers@andrew.cmu.edu,
choset@cs.cmu.edu

ABSTRACT

Robot system models often have difficulty allowing for direct command over all input degrees of freedom if the system has a large number of imposed constraints. A snake robot with more than three links and a nonholonomic wheel on each link cannot achieve arbitrary configurations in all of its joints simultaneously. For such a system, we assume partial command over a subset of the joints, and allow the rest to evolve according to kinematic chained and dynamic models. Different combinations of commanded and passive joints, as well as the presence of dynamic elements such as torsional springs, can drastically change the coupling interactions and stable oscillations of the joints. We use the oscillation modes that emerge to inform feedback controllers that achieve desired overall locomotion of the robot.

INTRODUCTION

A common design for a multi-link snake robot, for example shown in Fig. 1, is to place nonholonomic wheels on each of the links, ensuring that resultant motion only occurs the body longitudinal direction. This allows for the development of relatively simple kinematic models that describe the coupling behaviors among the joints and the overall locomotion of the robot. While one often assumes control via motors in each individual joint, the kinematic models restrict the set of valid input trajectories, prescribing the robot to follow shapes such as a serpenoid curve [1] in order to avoid singular configurations or those for which the constraints cannot be satisfied exactly.

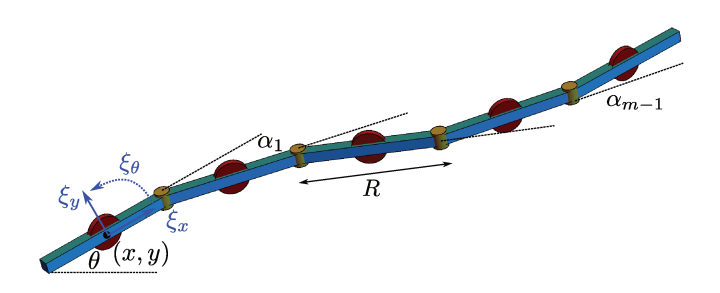


FIGURE 1. A *m*-LINK NONHOLONOMIC SNAKE ROBOT. THE COORDINATES (x,y,θ) DENOTE THE INERTIAL CONFIGURATION OF THE PROXIMAL LINK, WHICH ALSO HAS BODY VELOCITIES (ξ_x,ξ_y,ξ_θ) . RELATIVE JOINT ANGLES STARTING FROM THE PROXIMAL LINK ARE DENOTED $(\alpha_1,\ldots,\alpha_{m-1})$.

An early implementation of this system was Hirose's Active Cord Mechanism Model 3 [1], for which the author presented a heuristically derived position controller. Krishnaprasad and Tsakiris [2] introduced the notion of nonholonomic kinematic chains, formalizing the snake robot's configuration as a principal bundle in which periodic "internal" joint angle trajectories are lifted via a connection to a geometric phase, or displacement, in the "external" position variables. Ostrowski and Burdick [3] considered specific gaits for a three-link robot, including those that induce "serpentine" and rotation motion.

A branch of later work relevant to this paper focused on developing feedback controllers for certain gaits and relaxed mechanism designs. Prautsch and Mita [4] and Prautsch et al. [5] pro-

^{*}Address all correspondence to this author.

posed a position controller with all joints required to be actuated and centered about zero, but the gaits could not be applied to a three-link robot due to singularities. Matsuno and Mogi [6], Matsuno and Suenaga [7], and Matsuno and Sato [8] developed the idea of a "redundancy controllable" system and associated position controllers using both kinematic and dynamic models. This allowed for a greater variety of gaits and locomotion, but required the removal of nonholonomic constraints along the mechanism where control was to be imposed. Their controllers were able to actively steer away from singular configurations.

The analysis in this paper considers the full nonholonomic snake robot with constraints on each link. We first review the derivation of the kinematic and dynamic models for this system. By limiting actuation to two joints and one joint in each respective case, we describe how singularities and locking behaviors arise due to relative phase relationships between the joints. With oscillatory joint behaviors, we propose preliminary feedback controllers on trajectory components that intuitively produce system locomotion based on geometric phase analysis. Finally, we consider the addition of torsional springs on passive joints, allowing for stability and control for the relative phases of the joints as an extension of our previous work with a dynamic three-link robot [9, 10].

KINEMATIC MODEL

The system shown in Fig. 1 is a visual representation of a five-link nonholonomic snake robot. A general *m*-link robot simply has the requisite number of links appended or removed as necessary. Each link has an identical length *R* and a nonholonomically constrained wheel at the center. The velocity constraints induce locomotion of the overall system when the joints are actuated and the links are subsequently rotated.

The robot's configuration is denoted $q \in Q = G \times B$, where the configuration space Q is a product of two distinct subspaces. For this system, $g = (x, y, \theta)^T \in G = SE(2)$ are Lie group variables specifying the position and orientation of the proximal link, and the joint angles $b = (\alpha_1, \dots, \alpha_{m-1})^T \in B = \mathbb{T}^{m-1}$ describe the links' relative orientations to one another. In this paper links are numbered 1 (proximal) through m (distal) and joints 1 through m-1, with joint i connecting links i and i+1.

The kinematics of the system are described by the set of nonholonomic constraints on the wheels, which prohibit motion perpendicular to each of the links' longitudinal directions. They can be written as m equations of the form

$$-\dot{x}_i \sin \theta_i + \dot{y}_i \cos \theta_i = 0, \tag{1}$$

where (\dot{x}_i, \dot{y}_i) is the velocity and θ_i is the inertial orientation of the *i*th link. These quantities can be computed recursively in order to express them as functions of q. Starting with the proximal link,

we have that $(x_1, y_1, \theta_1) = (x, y, \theta)$; for i = 2, ..., m,

$$\theta_{i} = \theta_{i-1} + \alpha_{i-1},$$

$$x_{i} = x_{i-1} + \frac{R}{2}(\cos \theta_{i-1} + \cos \theta_{i}),$$

$$y_{i} = y_{i-1} + \frac{R}{2}(\sin \theta_{i-1} + \sin \theta_{i}).$$
(2)

The constraint equations are symmetric with respect to the group part G of the configuration, since the kinematics do not explicitly depend on where the system is positioned or how it is oriented in space. Q can thus be described formally as a *principal fiber bundle* [11] with the fibers G over the base manifold B. In such a structure, trajectories specified only in the base or shape space B can be mapped to trajectories in the position space G.

In order to find such a mapping, we can rewrite the constraints in a reduced Pfaffian form as

$$\omega_{\xi}(b)\xi + \omega_b(b)\dot{b} = 0, \tag{3}$$

where $\omega_{\xi} \in \mathbb{R}^{m \times 3}$, $\omega_b \in \mathbb{R}^{m \times (m-1)}$, and $\xi = (\xi_x, \xi_y, \xi_\theta)^T$ are the fiber velocities of the system expressed in a frame attached to the proximal link, as shown in Fig. 1. These "body velocities" can be viewed as a transformation of the inertial group velocities $\dot{g} = (\dot{x}, \dot{y}, \dot{\theta})$ to the tangent space at the identity element e of G. This mapping is formally expressed as $\dot{g} = T_e L_g \xi$, where $T_e L_g$ is the *lifted left action* given by

$$T_e L_g = \begin{pmatrix} \cos \theta - \sin \theta & 0 \\ \sin \theta & \cos \theta & 0 \\ 0 & 0 & 1 \end{pmatrix}.$$

Typically, one assumes that input commands are sent to the joint variables b. For a three-link robot (m-1=2), the number of constraints concides exactly with the dimension of the fiber. By specifying trajectories in both joint variables, fiber trajectories are then determined exactly by the constraint equations. For m > 3, however, each additional joint degree of freedom is added along with a new constraint on the overall system's motion. We can therefore arbitrarily control at most two joint degrees of freedom if all the constraints are to hold.

In this section we assume exactly two input degrees of freedom at any given time, denoted as $b_c = (\alpha_i, \alpha_j)^T$. The rest of the joint variables are denoted b_p and evolve passively according to the constraints. Eq. (3) can then be solved as

$$\xi = -A(b)\dot{b}_c,$$

$$\dot{b}_p = B(b)\dot{b}_c.$$
(4)

Here we explicitly separate the mappings from \dot{b}_c to ξ and \dot{b}_p , as A(b) is the *local connection form*, a base-valued mapping that lifts trajectories in the base to the fiber. Note that the Jacobian relationship between the commanded joint velocities \dot{b}_c and the passive ones \dot{b}_p takes on a similar linear form. Eq. (4) can be further simplified into a chained form as follows.

Proposition 1. *Suppose that* $b_c = (\alpha_i, \alpha_j)^T$ *where* i < j. *Then*

$$\dot{\alpha}_{k} = \begin{cases} f_{k}(\alpha_{k}, \alpha_{k+1}, \dots, \alpha_{j-1}, \alpha_{j}) \dot{b}_{c}, & k < i; \\ f_{k}(\alpha_{i}, \alpha_{i+1}, \dots, \alpha_{k-1}, \alpha_{k}) \dot{b}_{c}, & k > j; \\ f_{k}(\alpha_{i}, \alpha_{i+1}, \dots, \alpha_{i-1}, \alpha_{j}) \dot{b}_{c}, & i < k < j. \end{cases}$$
(5)

The kinematics of link k can then be extended from the joint velocity $\dot{\alpha}_k$. In particular, the kinematics of the proximal link (k = 1) can be written as

$$\xi = -A(\alpha_1, \alpha_2, \dots, \alpha_{j-1}, \alpha_j) \dot{b}_c. \tag{6}$$

Proof. Due to the recursive nature of how the constraint equations are defined, one can algebraically show that the constraint matrices in Eq. (3) have the forms

$$egin{aligned} \omega_{\xi} &= egin{pmatrix} 0 & 1 & 0 \ -\sinlpha_1 & \coslpha_1 & f(lpha_1) \ -\sin(lpha_1+lpha_2) & \cos(lpha_1+lpha_2) & f(lpha_1,lpha_2) \ dots & dots & dots \ -\sin\left(\sum_{l=1}^{m-1}lpha_l
ight)\cos\left(\sum_{l=1}^{m-1}lpha_l
ight)f(lpha_1,\ldots,lpha_{m-1}) \end{pmatrix}, \ \omega_b &= egin{pmatrix} 0 & 0 & 0 & \cdots & 0 \ R/2 & 0 & 0 & \cdots & 0 \ R/2 & 0 & 0 & \cdots & 0 \ f(lpha_2) & R/2 & 0 & \cdots & 0 \ f(lpha_2,lpha_3) & f(lpha_3) & R/2 & \ddots & dots \ dots & dots & dots & dots & dots & dots \ f(lpha_2,\ldots,lpha_{m-1}) & f(lpha_3,\ldots,lpha_{m-1}) & \ldots & f(lpha_{m-1}) & R/2 \ \end{pmatrix}. \end{aligned}$$

The kth line of either matrix, which corresponds to the kth constraint equation, only has dependencies on the joint angles $\alpha_1, \ldots, \alpha_{k-1}$. Furthermore, the first j+1 lines of the matrices yield j+1 independent equations. These equations are linear in the body velocities $(\xi_x, \, \xi_y, \, \xi_\theta)$ as well as the joint velocities $(\dot{\alpha}_1, \ldots, \dot{\alpha}_j)$. Given that we have command over two of them, this leaves us with j+1 unknown velocity quantities (three fibers plus j-2 joints), which can be linearly solved.

We now have a solution for the joint velocities $\dot{\alpha}_k$ with k < j. The kinematic maps for these solutions have dependencies from

 α_1 to α_j only, since no equations past the first j+1 rows of the constraint matrices are used. This thus proves Eq. (6). We can now solve for the joint velocities k>j by successively using each of the constraint equations in order starting from row j+2 of the constraint matrices. Each equation has dependencies up to α_k and introduces one unknown joint velocity $\dot{\alpha}_k$, which can be solved since the previous velocities are already known.

We now know that the kinematics must be of the form

$$\dot{\alpha}_k = \begin{cases} f_k(\alpha_1, \dots, \alpha_j) \dot{b}_c, & k < j; \\ f_k(\alpha_1, \dots, \alpha_k) \dot{b}_c, & k > j. \end{cases}$$
 (7)

A symmetry argument can be applied. Our choices of the proximal link and the joint α_1 are arbitrarily defined, with the physical kinematics of the system being unchanged if we had instead chosen to start α_1 from the distal link. Therefore, by defining the constraints relative to that link and going through the same procedure as above, we would obtain (in the original coordinates)

$$\dot{\alpha}_k = \begin{cases} f_k(\alpha_k, \dots, \alpha_{m-1}) \dot{b}_c, & k < i; \\ f_k(\alpha_i, \dots, \alpha_{m-1}) \dot{b}_c, & k > i. \end{cases}$$
 (8)

In order for both Eqs. (7) and (8) to simultaneously hold, the dependencies must only occur in their intersection. In other words, the function f_k has a dependency on α_l only if this is true in both equations. Eq. (5) can then be proved by applying this observation to each joint velocity in turn.

Adjacent Commanded Joints

Three-Link Robot. In considering the overall locomotion of the multi-link snake robot, we first take the case in which the two commanded joints are adjacent to each other, *i.e.*, $b_c = (\alpha_i, \alpha_{i+1})^T$. Due to the chained form of the kinematics, the evolution of the passive joint variables increases in complexity as they get farther away from α_i or α_{i+1} . We first review previous work regarding the simplest relevant configuration for this case, the three-link robot. For this system, one assumes command of both joint variables α_1 and α_2 ; there are no remaining passive joints. Then the kinematic mapping for ξ can be written as

$$\xi = -\frac{1}{D} \begin{pmatrix} \frac{R}{2} (\cos \alpha_1 + \cos(\alpha_1 - \alpha_2)) & \frac{R}{2} (1 + \cos \alpha_1) \\ 0 & 0 \\ \sin \alpha_1 + \sin(\alpha_1 - \alpha_2) & \sin \alpha_1 \end{pmatrix} \begin{bmatrix} \dot{\alpha}_1 \\ \dot{\alpha}_2 \end{bmatrix},$$
(9)

where $D = \sin \alpha_1 + \sin(\alpha_1 - \alpha_2) - \sin \alpha_2$. The second row, corresponding to ξ_y , is zero since this corresponds to the direction prohibited by the wheel of the proximal link. Note that Eqn. (9) also describes the fiber motion of a general m-link robot and is a reduced form of Eqn. (6). If α_1 and/or α_2 are not the commanded

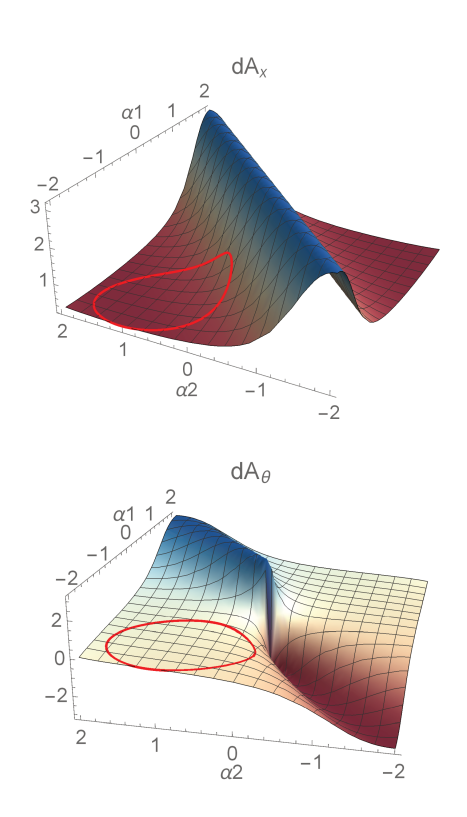


FIGURE 2. VISUALIZATIONS OF THE x AND θ COMPONENTS OF THE CONNECTION EXTERIOR DERIVATIVE FOR THE THREE-LINK SNAKE ROBOT.

joints when m > 3, one can use Eqn. (5) to first solve for these trajectories in terms of the controlled ones, and then apply Eqn. (9) to find the overall fiber motion. This is equivalent to solving Eqns. (5) and (6) simultaneously.

The quantity D is not well defined when $\alpha_1 = \alpha_2$, which corresponds to a singular configuration for the system. In this situation, we no longer have three independent constraints, so that two of them are insufficient to prescribe the three fiber degrees of freedom. We emphasize that this artifact does not mean that the robot is prohibited from being singular; that it arises here simply means that the kinematic model cannot tell us the fiber displacement of the robot when moving the joint angles into or from this configuration. A dynamic system model can bypass this problem if only one joint is commanded instead of two. For general operation of a multi-link robot with two commanded joint inputs, we will prefer gaits that avoid this and other singular configurations.

The structure of the Jacobian-like connection form in Eqn. (9) can be visualized in order to understand the response of ξ to input trajectories without regard to time [12]. By integrating each row of Eqn. (9) over a given joint trajectory, one can obtain a measure of displacement corresponding to the body frame directions. In the world frame, this measure provides the exact

rotational displacement, *i.e.*, $\dot{\theta} = \xi_{\theta}$ for the third row, and an approximation of the translational component for the first two rows. Assuming that we have periodic trajectories, or gaits, the integral can be realized by Stokes' theorem as

$$-\int_0^T A(b(\tau))\dot{b}(\tau)\,d\tau = -\int_{\Psi} A(b)\,db = -\int_{\mathcal{B}} \mathrm{d}A(b)\,db.$$

We can first convert the time integral to a line integral over the trajectory $\psi:[0,T]\to B$ in the joint space, since the kinematics are independent of input pacing. The second transformation is to an area integral over β , the region of the joint space enclosed by ψ . The integrand in the rightmost integral is the exterior derivative of A and is computed as the curl of A in two dimensions. For example, the connection exterior derivative of Eqn. (9) has three components, one for each row j given by

$$\mathrm{d}A_j(b) = rac{\partial A_{j,2}}{lpha_1} - rac{\partial A_{j,1}}{lpha_2}.$$

The magnitudes of the connection exterior derivative over the joint space are depicted in Fig. 2^1 , along with a gait trajectory shown as a closed curve on the surfaces. The area integral over the enclosed region is the geometric phase, a measure of the expected displacement in the body x and θ directions (the body y plot is not shown because it is zero everywhere). The x plot is positive everywhere, meaning that any closed loop will lead to net displacement along the ξ_x direction. The θ plot is antisymmetric about $\alpha_1 = -\alpha_2$, meaning that gaits symmetric about this line will yield zero net reorientation while simultaneously moving the robot forward. Note that the magnitudes in both plots become unbounded closer to the singular configurations $\alpha_1 = \alpha_2$.

Locked Passive Joint. Our analysis for a three-link robot helps us understand the types of gaits that would emerge for a robot with more than three links, where the commanded joints are α_i and α_{i+1} and the ones on either side of them are passive. In general, the kinematics of a joint α_{i+2} (or α_{i-1} by symmetry) for two adjacent commanded joints α_i and α_{i+1} are given by

$$\dot{\alpha}_{i+2} = \frac{\cos(\frac{1}{2}\alpha_{i+2})}{\sin(\frac{1}{2}(\alpha_{i} - \alpha_{i+1}))} \left(\frac{\sin(\frac{1}{2}(\alpha_{i+1} - \alpha_{i+2}))}{\cos(\frac{1}{2}\alpha_{i})} \dot{\alpha}_{i} - \frac{\sin(\frac{1}{2}(\alpha_{i} - 2\alpha_{i+1} + \alpha_{i+2}))}{\cos(\frac{1}{2}\alpha_{i+1})} \dot{\alpha}_{i+1} \right) \triangleq B_{i+2} \begin{bmatrix} \dot{\alpha}_{i} \\ \dot{\alpha}_{i+1} \end{bmatrix}. (10)$$

¹We plot a scaled arctangent of these functions in order to visualize the singular portions. Instead of $dA_i(b)$, we plot $\frac{1}{k} \arctan(kdA_i(b))$, where k is positive.

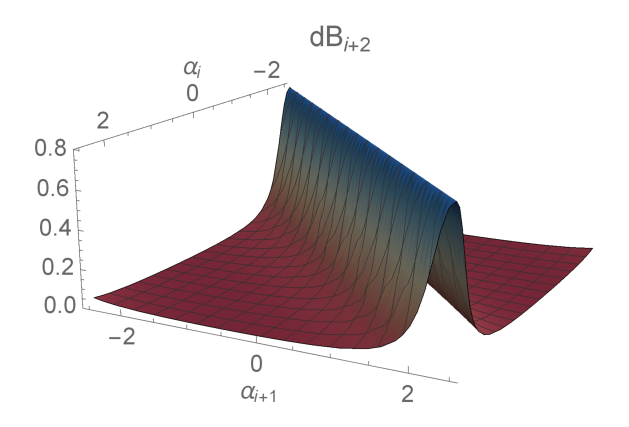


FIGURE 3. THE JACOBIAN EXTERIOR DERIVATIVE OF $\dot{\alpha}_{i+2}$ WHEN α_{i+2} IS NEAR BUT LESS THAN π .

An immediate observation is that $\alpha_{i+2} = \pm \pi$ are equilibria, as $\dot{\alpha}_{i+2}$ is zero at these configurations. This corresponds to the passive joint rotating all the way around such that link i+2 coincides with link i+1, normally an undesirable behavior. In the absence of dynamic mechanisms such as a torsional spring holding α_{i+2} near zero, we must ensure that the equilibrium at π is unstable, *i.e.*, $\dot{\alpha}_{i+2}$ should be negative if $\alpha_{i+2} = \pi - \varepsilon$ and positive if $\alpha_{i+2} = -\pi + \varepsilon$, where ε is a small positive number. It can be shown that Eqn. (10) is simply negated when between the two cases, so any solution that causes one equilibrium to be unstable will also be sufficient for the other.

In the same way that we visualize the exterior derivative of the connection form from Eqn. (9), we can do the same with the Jacobian B_{i+2} of Eqn. (10). By plotting the magnitude of the curl of B_{i+2} , we can see whether a given combination of α_i and α_{i+1} pushes α_{i+2} toward or away from $\pm \pi$. This is shown as the surface in Fig. 3 for $\alpha_{i+2} = \pi - \varepsilon$, where ε is a small positive number (again, this would be negated for $\alpha_3 = -\pi + \varepsilon$). While the absolute magnitudes are not important, it is clearly positive everywhere. Any closed loop that is traversed in a *counterclockwise* direction on the surface will yield a positive net area, pushing α_{i+2} toward π . In order to obtain the opposite result, we must have gaits corresponding to *clockwise* loops, which integrate to negative values and push α_{i+2} away from π . In the α_i - α_{i+1} space, clockwise loops are those in which α_{i+1} leads α_i ; i.e., their phase difference is between 0 and π .

Fig. 4 shows two simulations for a four-link robot verifying our conclusion. The commanded inputs (dashed lines) are $\alpha_1 = 0.3\cos(t) + 0.4$ and $\alpha_2 = 0.3\cos(t + \phi) - 0.4$, where $\phi = \frac{\pi}{6}$ in the first simulation, causing α_2 to lead α_1 , and $\phi = \frac{4\pi}{3}$ in the second, so that α_2 lags α_1 . In the former case, the passive response of α_3 (solid line) is pushed away from π , even though it starts out very

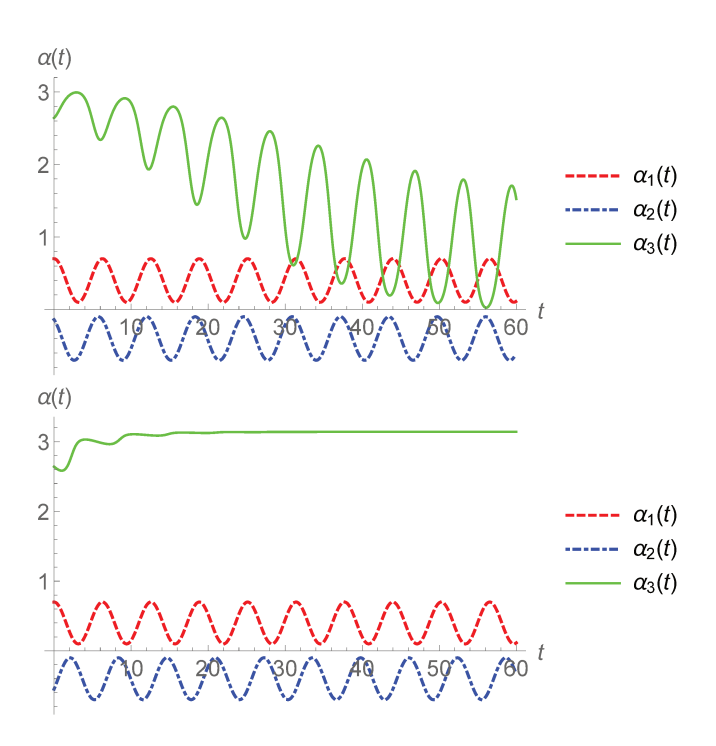


FIGURE 4. TRAJECTORIES OF COMMANDED INPUTS α_1 AND α_2 , AND THE PASSIVE RESPONSE α_3 . THE INPUTS' RELATIVE PHASE DETERMINES THE CONVERGENT BEHAVIOR OF α_3 .

close to that configuration and is even initially drawn to it before the end of the first gait cycle. The opposite is true in the second plot, in which α_3 converges to π and stays there throughout.

Oscillating Passive Joints. Assuming that α_i and α_{i+1} are prescribed so that the adjacent passive joint α_{i+2} does not lock up, α_{i+2} will have a steady-state oscillatory response. From the first plot of Fig. 4, we see that α_3 converges toward a trajectory that is nearly completely out of phase with α_2 . This observation holds exactly if α_{i+2} intersects α_{i+1} anywhere along its steady-state trajectory, *i.e.*, $\alpha_{i+2} = \alpha_{i+1}$, as Eqn. (10) reduces to $\dot{\alpha}_{i+2} = -\dot{\alpha}_{i+1}$. This means that the two trajectories are out of phase with each other.

Based on simulations and a linearization analysis of Eqn. (10), we make the following observations about the oscillatory response of α_{i+2} due to sinusoidal inputs with the same frequency but possibly different phase. We assume that ϕ is between 0 and π so that α_{i+2} does not end up locking. We also assume that the magnitues and offsets are such that the two trajectories do not cross to avoid singular configurations.

1. The magnitude of α_{i+2} depends on ϕ . When the commanded joints are in-phase, the passive joint has a range of about $A_i + A_{i+1}$. Otherwise, it is about the same magnitude as the

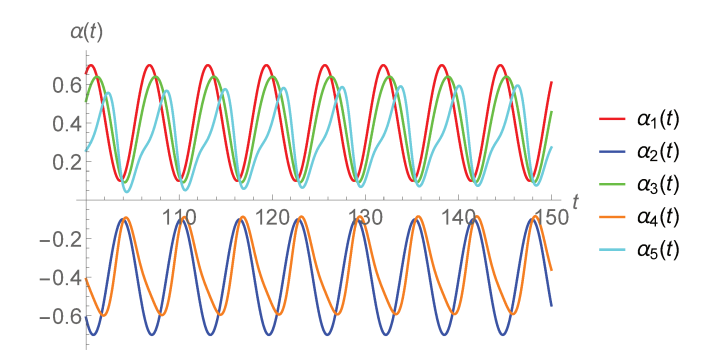


FIGURE 5. TRAJECTORIES OF COMMANDED INPUTS α_1 AND α_2 , AND THE PASSIVE RESPONSE OF JOINT ANGLES α_3 TO α_5 .

smaller of α_i and α_{i+1} .

- 2. α_{i+2} operates nearly out of phase to α_{i+1} , regardless of the original phase ϕ .
- 3. The offset of α_{i+2} is closer to that of α_i than α_{i+1} , so that the robot configuration tends toward a "zig-zag" shape.

These observations can be carried over to passive joints beyond α_{i+2} . Although the kinematics of an arbitrary joint α_i become increasingly complex and depend on all of the joints preceding it, the principal response of α_i is to move "opposite" to α_{i-1} . Thus, a natural mode of locomotion is that each successive joint trajectory alternates between the two forms set by the commanded joints, with slight decays in magnitude, phase, and offset going down the links. Fig. 5 depicts the trajectories of three passive joints in response to out-of-phase inputs to α_1 and α_2 . The first passive joint α_3 follows a trajectory close to α_1 , while leading α_2 by about the same phase that α_2 leads α_1 . The same statements can be made for α_4 and α_5 , each relative to the preceding joints. Note that the magnitudes and sinusoidal form increasingly decay as we move down the chain, since each passive joint does not perfectly replicate the opposite gait of the preceding one. A snapshot of the robot's configuration during these joint trajectories is shown in Fig. 6. This zig-zag shape is maintained throughout the locomotion of the robot.

We can make several statements about the overall locomotion of the robot in the plane as a result of different joint interactions. First, because the kinematics are of a chained form, the presence of links and passive joints beyond the standard three-link case does not change the locomotion of the proximal link if α_1 and α_2 are the commanded joints. Second, commanding joints in the interior of the robot, *i.e.*, joints that are neither α_1 nor α_{m-1} , is to be avoided in order to prevent an adjacent passive joint from locking at π . If α_i leads α_{i+1} , α_{i+2} will lock, as per our earlier conclusion; if the opposite is true, α_{i+1} leads α_i and so α_{i-1} will lock. Finally, the case that is left is if the two commanded joints are located at the distal links, which can be

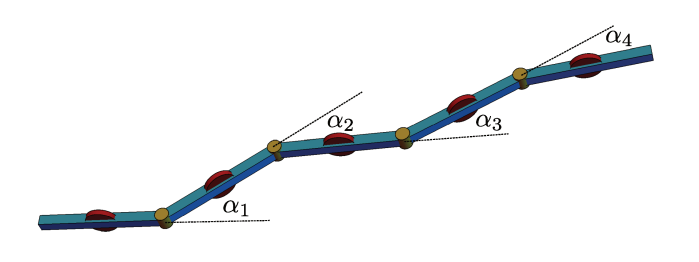


FIGURE 6. DEPICTION OF THE NATURAL "ZIG-ZAG" CONFIGURATION ACHIEVED BY THE PASSIVE JOINTS (α_3 AND α_4) OF A FIVE-LINK SNAKE ROBOT.

trivially solved by applying symmetry to find the joint responses starting from α_{m-1} down to α_1 .

Non-Adjacent Commanded Joints

The analysis of the previous subsection can be extended to situations in which the commanded subset of joints is arbitrary. Whereas having two adjacent controlled joints means that they have to be either (α_1, α_2) or (α_{m-1}, α_m) , making the robot's locomotion as a whole equivalent to that of a three-link robot, no such restriction exists when there are passive joints between the commanded ones. The kinematics of a passive joint α_i between two commanded ones α_{i-1} and α_{i+1} are given by

$$\dot{\alpha}_{i} = \frac{\cos(\frac{1}{2}\alpha_{i})}{\sin(\frac{1}{2}(\alpha_{i-1} - 2\alpha_{i} + \alpha_{i+1}))} \left(\frac{\sin(\frac{1}{2}(\alpha_{i} - \alpha_{i+1}))}{\cos(\frac{1}{2}\alpha_{i-1})}\dot{\alpha}_{i-1} + \frac{\sin(\frac{1}{2}(\alpha_{i} - \alpha_{i-1}))}{\cos(\frac{1}{2}\alpha_{i+1})}\dot{\alpha}_{i+1}\right) \triangleq B_{i} \begin{bmatrix} \dot{\alpha}_{i-1} \\ \dot{\alpha}_{i+1} \end{bmatrix}.$$
(11)

The form of this equation shares some similarities with Eqn. (10). However, in addition to again having undesired equilibria at $\alpha_i \pm \pi$, it is now also possible for the robot to passively find itself in a singular configuration if the sine term in the denominator goes to zero. Note that the singularities here are of a different nature from those of Eqn. (10), which correspond to the two commanded or adjacent joints having equal values. In that case, the inputs can directly be chosen to avoid those configurations. Here, in Eqn. (11) a singular configuration is one in which $\alpha_i = \frac{1}{2}(\alpha_{i-1} + \alpha_{i+1})$, the left-hand side being a quantity that we do not directly control.

Valid gaits are those that would push α_i away from the aforementioned value when it is near it. As before, we can visualize the Jacobian B_i of Eqn. (11), shown in Fig. 7 for $\alpha_i = \frac{1}{2}(\alpha_{i-1} + \alpha_{i+1}) - \varepsilon$, where ε is again a small positive number.

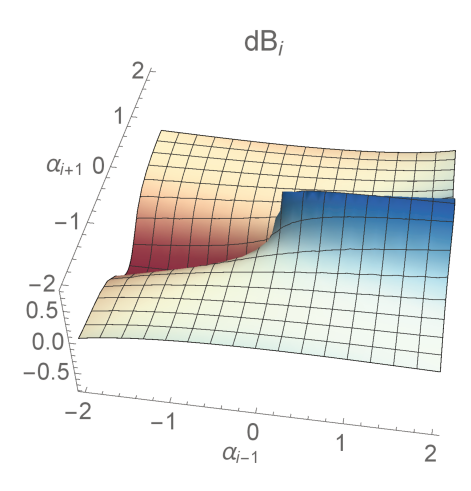


FIGURE 7. THE JACOBIAN EXTERIOR DERIVATIVE OF $\dot{\alpha}_i$ FOR $\alpha_{i+2} \approx \frac{1}{2}(\alpha_{i-1} + \alpha_{i+1})$.

Since we would like α_i to decrease and therefore a net negative area to be enclosed, a loop lying mostly above the $\alpha_{i-1} = \alpha_{i+1}$ line (upper left side of the plot) should run counterclockwise, and vice-versa for a gait below that line. While the sign of the net enclosed area may not be clear from inspection alone and require integration for gaits in which α_{i-1} and α_{i+1} are close in value, a rule of thumb is that the trajectory whose average value is smaller should be leading the other.

Fig. 8 shows the joint trajectories for a four-link robot, in which α_1 and α_3 are controlled and α_2 is passive. In both simulations, $\alpha_1(t) = 0.3\cos(t) + 0.4$ and $\alpha_3(t) = 0.3\cos(t+\phi) + 0.5$, with $\phi = -\frac{\pi}{3}$ in the first and $\phi = \frac{\pi}{3}$ in the second. In the first case, the "smaller" α_1 trajectory leads α_3 , so that α_2 is not attracted into the singular configuration and instead settles into an oscillatory trajectory opposite the trajectories on either side of it. This is consistent with what we found in Fig. 5, in which the roles of α_2 and α_3 are switched but the trajectories remain similar. However, when α_3 is made to lead α_1 in the second plot of Fig. 8, we have that α_2 is attracted to the value of $\frac{1}{2}(\alpha_1 + \alpha_3)$ at t = 2.9, at which point the kinematic model becomes infeasible.

If we have a valid gait trajectory that can avoid singular configurations, the general characterizations of the passive joint behaviors in the previous subsection can be applied here to inform a rudimentary feedback controller for locomotion. For example, suppose that we have a four-link robot in which the two outer joints α_1 and α_3 are commanded and the inner joint α_2 is passive. Since we know that locomotion of the proximal link can be found from α_1 and α_2 only (Eqn. (9)), we can achieve desired α_1 and α_2 trajectories by fixing α_1 and then "shaping" α_2 using α_3 . The qualitative aspects of a shaping controller are as follows.

1. The phase of α_2 is approximately the average of the phases of α_1 and α_3 , plus an additional π offset.

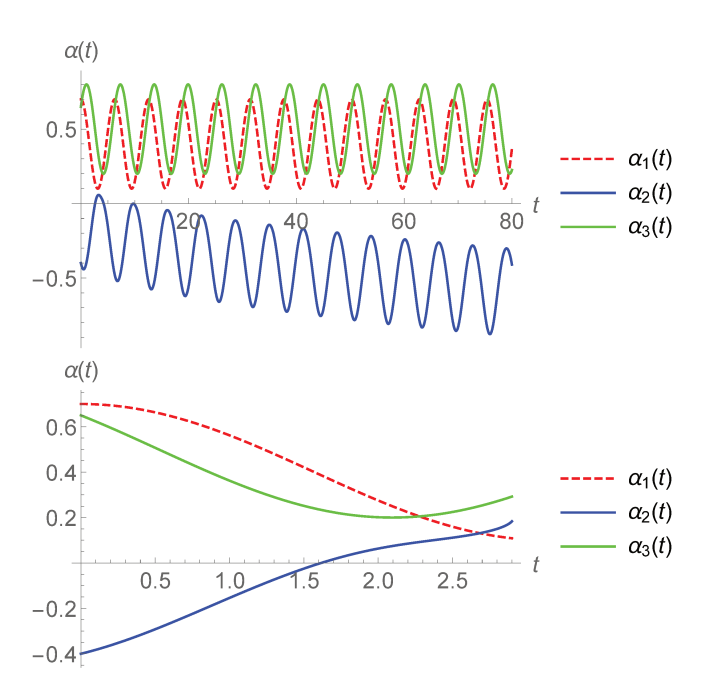


FIGURE 8. TRAJECTORIES OF COMMANDED INPUTS α_1 AND α_3 , AND THE PASSIVE RESPONSE α_2 . THE INPUTS' RELATIVE PHASE DETERMINES THE CONVERGENT BEHAVIOR OF α_2 .

- 2. The offset of α_2 depends on its initial value, but can be changed by shifting the offset or magnitude of α_3 relative to α_1 in the opposite direction.
- 3. The magnitude of α_2 is determined largely by its phase with respect to the commanded joints. A larger magnitude can be achieved by scaling α_3 proportionally when the trajectories are close to in-phase.

Given a fixed trajectory α_1 and a desired trajectory for α_2 , we can use the above guidelines to impose proportional or more complex feedback controllers on the parameters of α_3 . However, these controllers do not necessarily always converge, since the ability to shape the passive joint is rigidly limited by the possibility of hitting singular configurations. For example, the offset of α_2 may not be so close to the other two trajectories that it intersects them, limiting how much control we have over its magnitude. The robustness and convergence of this or an improved controller will be considered in future work.

In the simulation of Fig. 9, we have fixed $\alpha_1(t)$, but we desire $\alpha_2(t)$ to be farther away from the origin with an offset a_d and a phase ϕ_2 . We thus set $\alpha_3(t) = \alpha_1(t - 2\phi_2) + a_3(t)$, where

$$a_3(t) = k_p \left(\frac{1}{2} (\alpha_1(t) - \alpha_2(t)) - a_d \right),$$

where k_p is the controller gain. As can be seen in the top left plot,

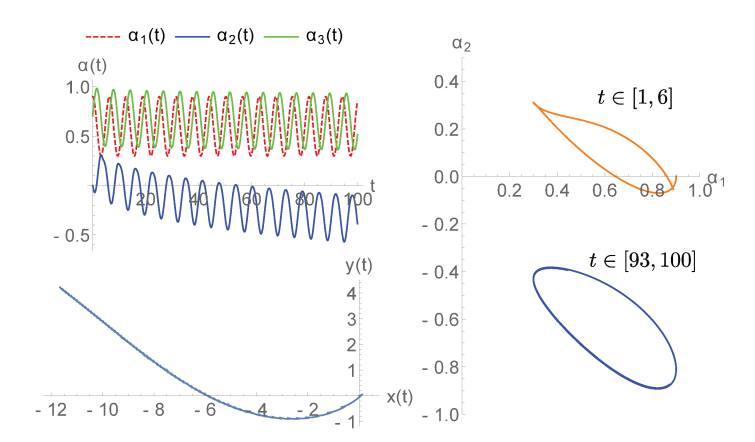


FIGURE 9. USING α_3 TO SHAPE α_2 OVER TIME (TOP LEFT) AND ACHIEVING A DESIRED TRAJECTORY IN THE α_1 - α_2 SPACE (RIGHT). BOTTOM LEFT: THE ROBOT'S FIBER MOTION.

the effect of the controller is to shrink α_3 (green) in magnitude and shift it downward over time. In response, α_2 (blue) decreases its offset away from α_1 and α_3 . The right plot shows a sampling of the trajectories in α_1 - α_2 space, where they are mostly elliptical loops starting near the α_1 axis (orange) and then eventually moving downward toward the $\alpha_1 = -\alpha_2$ line (blue). Finally, from the robot's connection derivative plots of Fig. 2, we know that these gaits will increase the reorientation of the robot from negative to zero, which is verified by the bottom left plot of the robot's fiber trajectory showing the change in curvature over time. If α_2 is further decreased, then the gaits become closer to the negative regions of dA_{θ} (shown as red in Fig. 2), which will cause the robot's trajectory to acquire the opposite curvature.

DYNAMIC MODEL

The kinematic model of the m-link robot has the advantage of being derived solely from the constraints, with each passive joint described by a first-order differential equation depending only on the joint angles between it and the commanded ones. However, this assumes that exactly two joints are commanded; if instead only one is commanded, then the m constraint equations are not sufficient to determine the m+1 degrees of freedom (m-2) passive joints plus three fibers). We have also seen that purely kinematic trajectories can be susceptible to joint locking, as well as singular configurations, such that the robot cannot execute arbitrary trajectories following the two prescribed inputs. Therefore, we turn to a full dynamic model in order to understand whether the robot can be designed or controlled in a way as to avoid these problems.

We assume that each link, indexed by i, has mass M_i and inertia J_i , in addition to the identical lengths R. Each joint, indexed by j, also has a mass M_j as well as spring constants k_j . The

last parameter allows us to place torsional springs on the passive joints; we assume that the resting configurations are all $\alpha_j = 0$. Now the Lagrangian of the whole system can be written as

$$L = \frac{1}{2} \sum_{i=1}^{m} \left(M_i (\dot{x}_i^2 + \dot{y}_i^2) + J_i \dot{\theta}_i^2 \right) + \frac{1}{2} \sum_{j=1}^{m-1} \left(M_j (\dot{x}_j^2 + \dot{y}_j^2) - k_j \alpha_j^2 \right), \tag{12}$$

where (x_i, y_i) and θ_i are the position and orientation of the *i*th link defined by Eqn. (2), and (x_j, y_j) is the position of the *j*th joint. If the body velocities ξ are substituted in for the inertial fiber velocities, then the Lagrangian can be reduced to a form

$$l(b, \xi, \dot{b}) = \frac{1}{2} \left[\xi^T \ \dot{b}^T \right] \tilde{M}(b) \begin{bmatrix} \xi \\ \dot{b} \end{bmatrix} - \frac{1}{2} \sum_{i=1}^{m-1} k_i \alpha_j^2, \tag{13}$$

where $\tilde{M}(b)$ is a *reduced mass matrix* with dependencies on the system parameters and joint angles only.

The second-order Euler-Lagrange equations of motion can then be derived, giving us three equations

$$\frac{d}{dt} \left(\frac{\partial l}{\partial \xi_{\{x,y,\theta\}}} \right) = \lambda(t) \omega_{\xi,\{x,y,\theta\}}$$
 (14)

and m-1 equations

$$\frac{d}{dt}\left(\frac{\partial l}{\partial \dot{\alpha}_{j}}\right) - \frac{\partial l}{\partial \alpha_{j}} = \lambda(t)\omega_{b,j} - d_{j}\dot{\alpha}_{j}.$$
 (15)

Here, $\omega_{\xi,\{x,y,\theta\}}$ and $\omega_{b,j}$ are the indicated columns of the constraint matrices in Eqn. (3), and $\lambda(t) = (\lambda_1(t), \dots, \lambda_m(t))$ is a horizontal vector of Lagrange multipliers corresponding to each of the constraints. Simple viscous dissipation terms $d_j \dot{\alpha}_j$ can be appended to the latter equations to ensure stability, where d_j are damping constants. Along with the constraint equations themselves, Eqns. (14) and (15) can be integrated in order to find the dynamic solutions of the robot.

The dynamical equations can be further reduced to the space of the joint variables only if desired. By solving the constraint equations along with Eqns. (14) and (15) as a linear system in the Lagrange multipliers, we can eliminate the $\lambda(t)$ variables and obtain a system in b only as

$$\tilde{M}_b(b)\ddot{b} + \tilde{C}(b,\dot{b}) + \tilde{K}(b) = 0. \tag{16}$$

These equations can then be analyzed for passive joint behaviors in response to commanded ones, without having to worry directly about the constraints or the fiber motion of the robot.

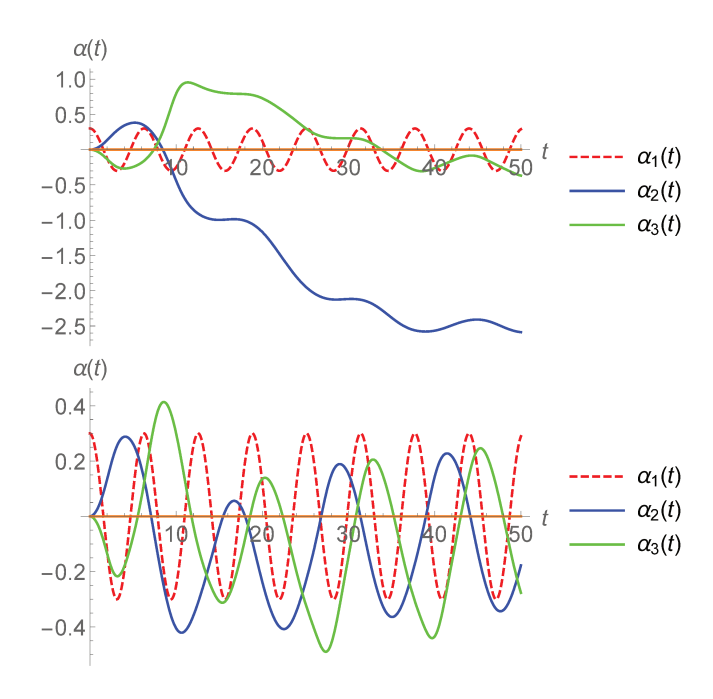


FIGURE 10. TOP: α_2 AND α_3 ARE COMPLETELY PASSIVE JOINTS, SO THAT THEY CAN DRIFT AWAY FROM THE ORIGIN. BOTTOM: α_2 AND α_3 HAVE STABILIZING SPRINGS.

The advantage to working with a dynamic model is that the robot's locomotion can be determined if only one joint is commanded. If two are commanded, then any resultant trajectories would ideally be identical to those determined by the kinematic model, but dynamics allow us to consider additional noise such as wheel slip close to singular configurations. If the kinematics are indeed modeled by "soft" rather than "hard" constraints to allow for wheel slip on arbitrary links, then it would be possible to allow for more than three commanded joints. The realization of soft constraints will be considered in future work; here we extend our work on a three-link robot with one commanded joint [9, 10] to a multi-link robot with the same.

In previous work we showed that singular configurations are not a problem with only one commanded joint; in fact, a natural response of the passive joint trajectories is such that they oscillate with the same offset as the commanded one. Since such gaits are mostly symmetric about the origin of the joint space, this allows for forward locomotion of the robot without net rotation. If the passive joints have nonzero spring constants, then these oscillations are stable. Fig. 10 shows two simulated trajectories, where $\alpha_1(t) = 0.3\cos(0.5t)$. All parameters are assigned to a value of 1 in both, except the spring constant on the passive joints k_2 and k_3 , which are 0 in the first plot. Without stabilizing springs, α_2 is able to drift away from the origin and would in fact converge toward π if damping were also nonexistent ($d_2 = 0$), a situation detrimental to overall locomotion. In contrast, when $k_2 = 1$ the

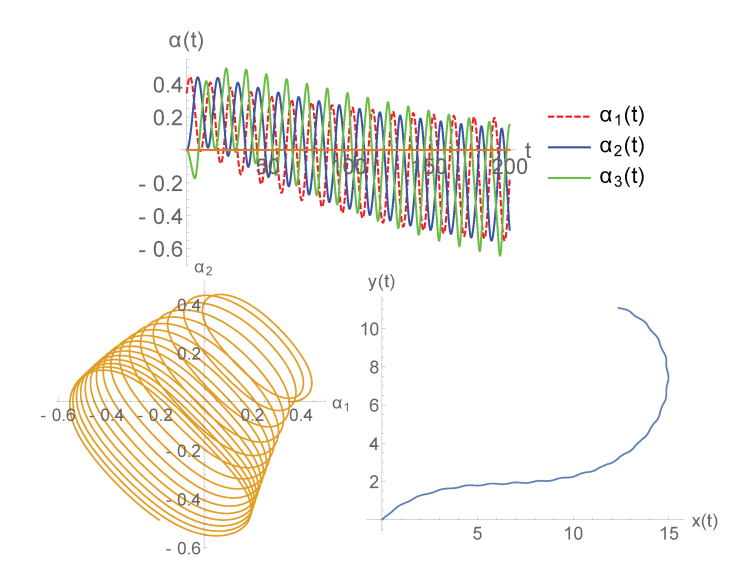


FIGURE 11. TOP: FEEDBACK-CONTROLLED TRAJECTORY OF α_1 AND PASSIVE RESPONSES OF α_2 AND α_3 . BOTTOM LEFT: THE TRAJECTORY IN α_1 - α_2 SPACE. BOTTOM RIGHT: THE ROBOT'S FIBER TRAJECTORY.

passive joints oscillate around α_1 with roughly equal phases.

Since singular configurations are not a problem, a stabilizing feedback controller can be more easily defined than in the kinematic case. First, a frequency sweep of the linearized passive joint dynamics reveals that they have a characterisic low-pass behavior. For lower frequencies of the input α_1 , or higher values of the spring constants k_j (thereby increasing the resonant frequencies), the joint responses have magnitude roughly equal to that of α_1 and are in-phase with each other. For higher input frequencies or less stiff springs, the joint trajectories become alternately out-of-phase and start to shrink in magnitude. This information thus informs selection of the appropriate input frequency for the desired phase of the passive joints.

If the commanded joint's offset and magnitude are changed in a continuous way, the passive joints generally follow those changes as well. Thus, gaits are roughly centered around $\alpha_1 \approx \alpha_2 \approx \cdots \approx \alpha_{m-1}$. This is sufficient for achieving arbitrary fiber motions on the plane, since we can use the kinematic model of geometric phase to approximate gaits that will mainly move the robot forward in the same body direction (centered about the origin), or those that turn the robot in a specific direction (offsetting the gait away from the origin). Feedback controllers, as described for the kinematic model, can then be imposed on the magnitude and offset of the input α_1 in order to achieve the same desired values for the passive joints. The net effect is to shift and shape the trajectory along the $\alpha_1 = \alpha_2$ line in joint space in order to achieve a desired displacement and reorientation per cycle.

Fig. 11 shows an example of this controller applied to a four-

link robot. The joint trajectories initially start centered around 0.2 radians, with a magnitude about the same. These are the loops centered around the second quadrant of the joint space plot (bottom left). The input frequency was chosen such that the phase is about a third of a gait cycle, so that the joints are all equal in phase to each other. As a result, the robot follows a trajectory of slightly negative curvature and with a small forward displacement per gait cycle (bottom right). It is then desired for the robot to start turning more sharply in the opposite direction—this corresponds to shifting the gait downward to the third quadrant in α_1 - α_2 space and increasing its magnitude. As shown in the top plot, this is achieved by increasing the magnitude and decreasing the offset of α_1 over time, causing both α_2 and α_3 to follow.

This controller design can be applied to robots with an arbitrary number of links. The passive joint trajectories will change since the presence of additional joints down the line couple into their dynamics. However, the commanded joint can still use feedback to shape the adjacent joint, followed by the remaining ones down the chain, with each successive one down the chain following its predecessor.

CONCLUSIONS AND FUTURE WORK

We have developed and studied kinematic and dynamic models for a *m*-link fully nonholonomic snake robot. With the kinematic model we showed that the joint kinematics take on a chained form, allowing us to determine gaits with two adjacent or non-adjacent joints that can avoid locked and singular configurations. We also characterized oscillatory modes for the passive joints that qualitatively inform a class of feedback controllers. The dynamic model, though more complex, allows for elements such as stabilizing torsional springs and locomotion of the robot by actuating only one joint. A feedback controller similar to the one developed in the kinematic case, but more robust due to the absence of singularities, was also demonstrated in order to intuitively achieve gaits in the joint space. These results were then discussed in relation to geometric phase analysis for a three-link robot in order to describe the robot's motion.

Going forward we would like to find more quantitative relationships among the various joints for both the kinematic and dynamic models. Although the differential equations cannot be solved exactly, a major step forward would be to analytically solve for features such as the phase of a passive joint given a particular input form. This would then lead to provably stabilizing feedback controllers that converge toward desired trajectories and away from singularities. With the dynamic model, we also plan to fully characterize the robot's fiber motion in terms of all the joints, as the kinematic model that only depends on the first two proximal joints is only an approximation when they are not commanded together. Another dynamic aspect that we plan to explore is that of wheel slip or lateral friction, which would likely be more faithful to a physical system. By "softening" the

constraints we can then extend our work to analogous kinematic systems such as a low or high Reynolds swimmer snake robot.

REFERENCES

- [1] Hirose, S., 1993. "Biologically inspired robot". *Oxford University Press*.
- [2] Krishnaprasad, P. S., and Tsakiris, D. P., 1994. "G-snakes: Nonholonomic kinematic chains on lie groups". In Decision and Control, 1994., Proceedings of the 33rd IEEE Conference on, Vol. 3, IEEE, pp. 2955–2960.
- [3] Ostrowski, J., and Burdick, J., 1996. "Gait kinematics for a serpentine robot". In Robotics and Automation, 1996. Proceedings., 1996 IEEE International Conference on, Vol. 2, IEEE, pp. 1294–1299.
- [4] Prautsch, P., and Mita, T., 1999. "Control and analysis of the gait of snake robots". In Control Applications, 1999. Proceedings of the 1999 IEEE International Conference on, Vol. 1, IEEE, pp. 502–507.
- [5] Prautsch, P., Mita, T., and Iwasaki, T., 2000. "Analysis and control of a gait of snake robot". *IEEJ Transactions on Industry Applications*, 120(3), pp. 372–381.
- [6] Matsuno, F., and Mogi, K., 2000. "Redundancy controllable system and control of snake robots based on kinematic model". In Decision and Control, 2000. Proceedings of the 39th IEEE Conference on, Vol. 5, IEEE, pp. 4791–4796.
- [7] Matsuno, F., and Suenaga, K., 2003. "Control of redundant 3d snake robot based on kinematic model". In Robotics and Automation, 2003. Proceedings. ICRA'03. IEEE International Conference on, Vol. 2, IEEE, pp. 2061–2066.
- [8] Matsuno, F., and Sato, H., 2005. "Trajectory tracking control of snake robots based on dynamic model". In Robotics and Automation, 2005. ICRA 2005. Proceedings of the 2005 IEEE International Conference on, IEEE, pp. 3029–3034.
- [9] Dear, T., Kelly, S. D., Travers, M., and Choset, H., 2016. "The three-link nonholonomic snake as a hybrid kinodynamic system". In 2016 American Control Conference (ACC), pp. 7269–7274.
- [10] Dear, T., Kelly, S. D., Travers, M., and Choset, H., 2016. "Locomotive analysis of a single-input three-link snake robot". In 2016 IEEE 55th Conference on Decision and Control (CDC), pp. 7542–7547.
- [11] Kelly, S. D., and Murray, R. M., 1995. "Geometric phases and robotic locomotion". *Journal of Robotic Systems*, 12(6), pp. 417–431.
- [12] Hatton, R. L., and Choset, H., 2011. "Geometric motion planning: The local connection, stokes theorem, and the importance of coordinate choice". *The International Journal of Robotics Research*, *30*(8), pp. 988–1014.